



2017-08-18

Reflectance of XUV Light on a Two Dimensional Conducting Rough Surface

Chelsea Thangavelu
clthangave@brynmawr.edu

Follow this and additional works at: <https://scholarsarchive.byu.edu/studentpub>

 Part of the [Physics Commons](#)

This paper was completed during the 2017 Research Experiences for Undergraduates in Physics (REU) program. More information about this program can be found [here](#).

BYU ScholarsArchive Citation

Thangavelu, Chelsea, "Reflectance of XUV Light on a Two Dimensional Conducting Rough Surface" (2017). *All Student Publications*. 211.
<https://scholarsarchive.byu.edu/studentpub/211>

This Report is brought to you for free and open access by BYU ScholarsArchive. It has been accepted for inclusion in All Student Publications by an authorized administrator of BYU ScholarsArchive. For more information, please contact scholarsarchive@byu.edu, ellen_amatangelo@byu.edu.

Reflectance of XUV Light on a Two Dimensional Conducting Rough Surface

Chelsea Thangavelu

August 18, 2017

Abstract

A Fortran program is set up to solve for the reflectance of XUV light from a rough two dimensional surface, resembling experimental mirrors used to reflect XUV light. Because the roughness of the surface is on the order of magnitude of the wavelength of XUV light, our approach requires a Greene's Function instead of using traditional geometrical optics or physical optics. Our Fortran program calculates the impedance (Z) matrix which requires integration over Greene's Function at non-singular points. The Z matrix helps solve for the induced surface current $J(\vec{x}')$ at non-singular points. At singular points, the program implements a series of transformations, including the Duffy transformation, in order to eliminate the singularities. This allows for integration of the Greene's Function over the rough surface using numerical Gaussian quadrature rules. The transformations lead to solving for weights specific to each singularity that aid in the calculation of $J(\vec{x}')$ at singular points. After an incident electric field is generated in the program, the scattered electric field can be solved for directly.

Contents

1	Introduction	3
2	Approach	3
2.1	Create Surface	6
2.2	Compute Non-Singular Impedance Matrix	7
2.3	Compute Impedance Matrix at Singularities	7
3	Results and Discussion	9
3.1	Circular Integration Rule	9
3.2	Surface Generation and Interpolation Using Splines	10
3.3	Using Transformations for Non-Singular Calculations	11
4	Conclusion	13

1 Introduction

Extreme ultraviolet radiation (XUV), a section of the electromagnetic spectrum, has wavelengths between 1 nm and 80 nm. Some applications of XUV include making precise images because of their relatively small wavelength, developing XUV plasma spectroscopy which helps characterize objects such as stars, and improving the resolution of lithography [1, 2]. Looking at XUV light emitting objects can be revealing but requires telescopes with mirrors that reflect XUV light. Because the roughness of a very smooth mirror is around the same order of magnitude as the wavelength of XUV radiation, reflectance cannot be predicted through traditional methods like geometrical optics or physical optics. Spatial frequency and root mean square (rms) roughness are parameters that help characterize roughness. Spatial frequency refers to how often bumps occur on a surface while rms roughness depicts the height of the peaks and grooves of a surface.

We approach this problem with a scalar electric field, one component of the vector field. Greene's function, which aids in calculating the reflectance of XUV light, in three dimensional space

$$G(\vec{x}, \vec{x}') = \frac{e^{ik|\vec{x}-\vec{x}'|}}{4\pi|\vec{x}-\vec{x}'|}, \quad (1)$$

where \vec{x} is the observation point and \vec{x}' is the source point, is a solution to the homogeneous Helmholtz equation[3]. It relates the electric field E to the induced current J :

$$E(\vec{x}) = \int J(\vec{x}')G(\vec{x}, \vec{x}')d\vec{x}'. \quad (2)$$

2 Approach

In the Fortran program, using a perfect conductor as the reflecting surface simplifies calculations because on such a conductor,

$$E_{tot} = 0 = E_i + E_r, \quad (3)$$

where E_i represents the electric field incident on the conductor and E_r represents the scattered electric field.

The Nyström Method converts the continuous equation 2 into a matrix equation so the induced surface current is solvable by means of matrix inversion. First, discretizing equation 2 yields

$$E(\vec{x}) \approx E_i = \sum_j G_{i,j}w_jJ_j \quad (4)$$

where E_i represents a column matrix of the values of the incident electric field at observation points i , or previously \vec{x} , along the surface. w_j and J_j represent column matrices of the weight determined by the cubature rule used and the value of the surface current respectively at source points j , or previously \vec{x}' . Equation 1, Greene's function, is calculated for all the observation points i and source points j to find the values of all the entries in the Greene's

Function matrix, $G_{i,j}$. The Nyström Method requires that the set of observation points are the same as the integration points. Next, let the impedance matrix

$$Z_{i,j} = G_{i,j}w_j \quad (5)$$

to simplify equation 4 to

$$E_i = \sum_j Z_{i,j}J_j. \quad (6)$$

The computer generates an incident electric field column matrix so that the only unknown in equation 6 is J_j . Equation 6 becomes a matrix equation after finding n places where the relationship holds true. This creates a set of n linear equations with n unknowns, making it possible to solve for J_j using matrix inversion; however, the electric field and the impedance matrix must be generated before solving for J_j .

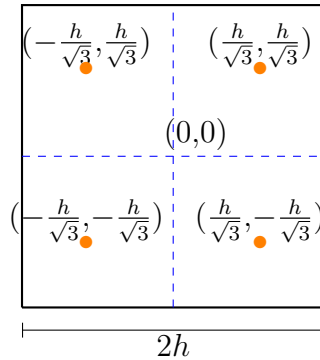


Figure 1: The square rule is shown with the origin at the center of the square with side $2h$ and points $(\pm \frac{h}{\sqrt{3}}, \pm \frac{h}{\sqrt{3}})$ [4].

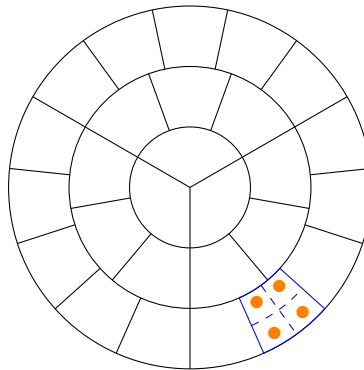


Figure 2: The patches used in the circular integration rule. Each patch has an equal area and each ring has a width a [5].

The numerical cubature rule, developed by Turley and depicted in Figure 2, serves as a tool in calculating the entries of $Z_{i,j}$ as it determines w_j in equation 5 [5]. The cubature rule maps the square rule [4] in Figure 1 onto a circle as shown in Figure 2. The square

rule numerically integrates a function over a square centered about the origin with side $2h$ by calculating the function at points $(\pm\frac{1}{3}\sqrt{3}h, \pm\frac{1}{3}\sqrt{3}h)$ and multiplying each function value at those points by a weight $w = \frac{1}{4}$ such that the integral I over a function $f(x, y)$ over the square is

$$I = \frac{1}{4} \sum f(\pm\frac{1}{3}\sqrt{3}h, \pm\frac{1}{3}\sqrt{3}h). \quad (7)$$

The circle that we map the square rule onto has a radius $s = a(N + 1)$ where a is the ring width, N is the number of rings, and n is the ring index starting at zero. Each ring has $3(2n + 1)$ segments such that each arc piece has the same area, facilitating the mapping of the square rule to the circular rule. Additionally splitting the rings into patches make calculations at singular points, where $x = x'$ in Greene's Function, more efficient. After mapping, the integration rule approximates that

$$\int_0^s r dr \int_0^{2\pi} f(r, \theta) d\theta \approx \frac{\pi a^2}{12} \sum_{n=0}^{N-1} \sum_{m=0}^{2n+2} 1 + \frac{1}{\sqrt{3}(2n+1)} [f(r_+, \theta_+) + f(r_+, \theta_-)] + 1 - \frac{1}{\sqrt{3}(2n+1)} [f(r_-, \theta_+) + f(r_-, \theta_-)] \quad [5] \quad (8)$$

where r_+, r_-, θ_+ , and θ_- are the maps of the four points from the square rule using $2h = a$

$$r_+ = a \left(n + \frac{1}{2} + \frac{1}{2\sqrt{3}} \right) \quad (9)$$

$$r_- = a \left(n + \frac{1}{2} - \frac{1}{2\sqrt{3}} \right) \quad (10)$$

$$\theta_+ = 2\pi \frac{(m + \frac{1}{2}) + \frac{1}{2\sqrt{3}}}{3(2n+1)} \quad (11)$$

$$\theta_- = 2\pi \frac{(m + \frac{1}{2}) - \frac{1}{2\sqrt{3}}}{3(2n+1)}, \quad (12)$$

and m and f represent the arc piece index, starting from zero in each ring, and the function to integrate over respectively [5].

A circular reflecting surface best suits this problem because the cornerless circle reduces edge effects and resembles the symmetry of the expected solution. Also, when we integrate over singular patches, where the singularities are caused by Greene's function, it is more efficient to have the rings split up into patches rather than left as whole rings.

The coefficients in the integration become the weights needed to fill the impedance matrix which allows us to solve for the induced surface current $J(\vec{x}')$ in equation 6. Once $J(\vec{x}')$ is known, the scattered electric field can be solved for by plugging $J(\vec{x}')$ into

$$E_r(\vec{x}) = - \int J(\vec{x}') G(\vec{x}, \vec{x}'). \quad (13)$$

2.1 Create Surface

To create the surface, normally distributed pseudo-random numbers fill a matrix representing the surface heights at each point (i, j) in the matrix. The Box-Muller Transform assists in generating these numbers by ensuring a normal distribution and a standard deviation of one [6]. The Fortran program randomly selects two numbers, U_1 and U_2 , between 0 and 1, each number having the same likelihood of being selected. Then, the Box-Muller transform,

$$z_1 = \sqrt{-2\ln(x_1)} \cos 2\pi U_2 \quad (14)$$

$$z_2 = \sqrt{-2\ln(x_1)} \sin 2\pi U_2, \quad (15)$$

returns two numbers, z_1 and z_2 , with a Gaussian distribution, an expectation value of zero, and a standard deviation of one.

After the pseudo-random heights selection, high spatial frequencies must be reduced to ensure a realistic surface, so a Fast Fourier Transform returns the amplitudes of each spatial frequency in the surface. Next, inputting the spatial frequencies into a half Gaussian

$$f(\nu) = e^{-\frac{\nu^2}{2\sigma^2}}, \quad (16)$$

where ν is the spatial frequency, filters out unrealistically high spatial frequencies. A half Gaussian works better than a hard frequency cut-off because it prevents ringing [7]. Additionally, atomic force microscopy data has shown that the power spectral density of an experimental mirror used to reflect XUV light resembles a half Gaussian as shown in Figure 3.

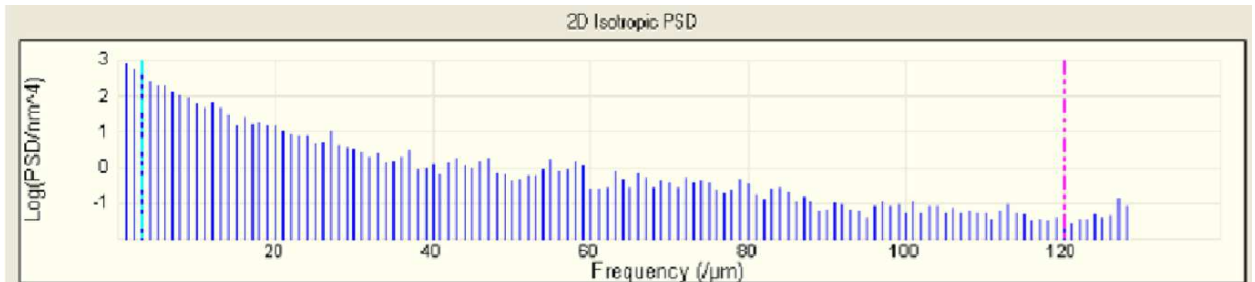


Figure 3: Power spectral density of mirror used in lab to reflect XUV light. Produced from atomic force microscopy data. Resembles half Gaussian [8].

A backwards Fast Fourier Transform returns the surface to the spatial domain where the height entries are divided by the rms roughness of the current surface

$$\Delta h = \sqrt{\langle h^2 \rangle - \langle h \rangle^2} \quad (17)$$

where $\langle h \rangle$ is the mean height

$$\langle h \rangle = \frac{h_i}{N}, \quad (18)$$

N is the number of heights, and $\langle h^2 \rangle$ is the mean of the square height. Finally, the product of these heights and the desired rms roughness returns a matrix of surface heights with the desired rms roughness.

2.2 Compute Non-Singular Impedance Matrix

Each entry of the impedance matrix correlates to the points specified in the circular integration rule in Figure 2. The matrix is calculated by

$$Z_{i,j} = w_j S_j G_{i,j} \quad (19)$$

where w is the weight specified by the integration rule in equation 7, S_j is a column matrix of the surface Jacobian

$$S = \sqrt{1 + \frac{\partial z^2}{\partial x} + \frac{\partial z^2}{\partial y}} \quad (20)$$

at each of the source points, and $G_{i,j}$ is the value of the Greene's function at the points specified in the circular integration rule, listed in equations 9, 10, 11, and 12. i and j refer to the observation and source points respectively and are different points for the non-singular case. In equation 20, $\frac{\partial z}{\partial x}$ and $\frac{\partial z}{\partial y}$ describe the partial derivatives of the height of the surface with respect to x and y . Equation 20 differs from equation 4 by a factor of S which takes into account the roughness of the surface when calculating each entry of the impedance matrix. Once the incident electric field is generated, solving the linear equation

$$E(\vec{x}) \approx E_i = \sum_j w_j Z_{i,j} S_j J_j \quad (21)$$

returns J_j .

2.3 Compute Impedance Matrix at Singularities

$G(\vec{x}, \vec{x}')$ in equation 1 is singular when $\vec{x} = \vec{x}'$. In order to address this problem, we treat impedance matrix elements where $\vec{x} = \vec{x}'$, or $i = j$, and where i and j are on the same patch differently. Instead of calculating the singular entries of the impedance matrix, we integrate over the product of Greene's function, the surface Jacobian, and one of four equations over which the circular integration rule is exact. We can calculate $J(\vec{x}')$ through the following system of four equations:

$$E(\vec{x}') \approx E_i = \sum c_j J_j \quad (22)$$

where the impedance matrix and surface Jacobian from equation 21 has been absorbed into c .

The four functions that we use in calculating c that can be integrated exactly are

$$f(r, \theta) = \begin{pmatrix} 1 \\ r \\ \theta \\ r\theta \end{pmatrix}, \quad (23)$$

so we have a column matrix of the exact integrals

$$\begin{pmatrix} \int S(\vec{x}')G(\vec{x}, \vec{x}')dA' \\ \int rS(\vec{x}')G(\vec{x}, \vec{x}')dA' \\ \int \theta S(\vec{x}')G(\vec{x}, \vec{x}')dA' \\ \int r\theta S(\vec{x}')G(\vec{x}, \vec{x}')dA' \end{pmatrix}. \quad (24)$$

When we plug in the points required by the circular integration rule from equations 9, 10, 11, and 12 into the functions in equation 23 on a given patch, we get a four by four matrix since there are four points on each patch and four functions to plug each point into:

$$W(r, \theta) = \begin{pmatrix} 1 & 1 & 1 & 1 \\ r_+ & r_+ & r_- & r_- \\ \theta_+ & \theta_- & \theta_+ & \theta_- \\ r_+\theta_+ & r_+\theta_- & r_-\theta_+ & r_-\theta_- \end{pmatrix}. \quad (25)$$

The matrix multiplication product of $W(r, \theta)$ and a column matrix containing coefficients c should be a column matrix of the exact integrals of the product of Greene's function and the surface Jacobian $S(\vec{x}')$ over each singular patch. We can solve for the weights necessary in calculating the impedance matrix entries at singular points by solving the matrix equation

$$\begin{pmatrix} 1 & 1 & 1 & 1 \\ r_+ & r_+ & r_- & r_- \\ \theta_+ & \theta_- & \theta_+ & \theta_- \\ r_+\theta_+ & r_+\theta_- & r_-\theta_+ & r_-\theta_- \end{pmatrix} \begin{pmatrix} c_1 \\ c_2 \\ c_3 \\ c_4 \end{pmatrix} = \frac{1}{a^2} \begin{pmatrix} \int S(\vec{x}')G(\vec{x}, \vec{x}')dA' \\ \int rS(\vec{x}')G(\vec{x}, \vec{x}')dA' \\ \int \theta S(\vec{x}')G(\vec{x}, \vec{x}')dA' \\ \int r\theta S(\vec{x}')G(\vec{x}, \vec{x}')dA' \end{pmatrix} \quad (26)$$

where the subscripts refer to the coordinates of the four different points on a given patch. Therefore, this equation must be solved for every patch in the circular integration region. We integrate over dA' or over the source points in the singular arc piece. After plugging in the values in equations 9, 10, 11, and 12, we find the solution c to this system of linear equations is

$$c_1 = \frac{1}{4\pi} (2(2 + \sqrt{3} + (3 + \sqrt{3})n + m(3 + \sqrt{3} + 6n))\pi W(r, \theta)_1 - 2(3 + \sqrt{3} + 6m)\pi W(r, \theta)_2 - 3(1 + 2n)(-6W(r, \theta)_4 + (3 + \sqrt{3} + 6n)W(r, \theta)_3))$$

$$c_2 = \frac{1}{4\pi} (2\pi((-1 + m(-3 + \sqrt{3} - 6n) - (3 + \sqrt{3})n)W(r, \theta)_1 + (3 + \sqrt{3} + 6m)W(r, \theta)_2 + 3(1 + 2n)(-6W(r, \theta)_4 + (3 - \sqrt{3} + 6n)W(r, \theta)_3))$$

$$c_3 = \frac{1}{4\pi}(-2(-2 + \sqrt{3} + m(-3 + \sqrt{3} - 6n) + (-3 + \sqrt{3})n)\pi W(r, \theta)_1 + 2(-3 + \sqrt{3} - 6m)\pi W(r, \theta)_2 + 3(1 + 2n)(6W(r, \theta)_4 + (-3 + \sqrt{3} - 6n)W(r, \theta)_3))$$

$$c_4 = \frac{1}{4\pi}(-2\pi((1 + 3n - \sqrt{3}n + m(3 + \sqrt{3} + 6n))W(r, \theta)_1 + (-3 + \sqrt{3} - 6m)W(r, \theta)_2) + 3(1 + 2n)(-6W(r, \theta)_4 + (3 + \sqrt{3} + 6n)W(r, \theta)_3))$$

where the indices in after c and $W(r, \theta)$ refer to the specific entries in the column matrices. Finally, we can calculate $J(\vec{x}')$ using equation 22.

In order to evaluate these integrals on the right side of equation 26, we must first eliminate the singularity using transformations. Specifically, we use the Duffy Transform which removes a singularity at the origin of a standard right triangle by transforming the triangle into a square, expanding the singularity into a line[9]. In order to transform the patches in the circular integration rule into a standard right triangle to prepare for a Duffy Transform, each patch is transformed into a square, and each square is divided into four triangles where all triangles share a vertex at the singularity as shown in Figure 4. Because there are four singularities on each patch, there are sixteen different transformations that transform each triangle into a standard right triangle.

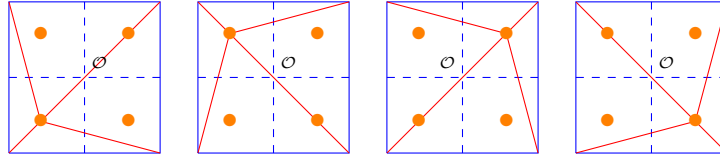


Figure 4: The Duffy Transform eliminates singularities at the origin when integrating over standard right triangles [9]. In order to use it, we transform the patches from the circular integration rule into a square and divide the square into triangles with the singularity at a vertex as shown below.

After eliminating the singularity, the Fortran program can evaluate the right side of equation 26 and therefore calculate the weights needed to calculate the induced surface current at those source points.

3 Results and Discussion

3.1 Circular Integration Rule

Figure 2 shows results of the circular integration rule in a Fortran program and compares it to exact answers from a Mathematica notebook. We integrate over different functions using different radii and numbers of rings. Because the circular integration rule returns an approximate integral, the returned value may not be the same as that from Mathematica. When integrating over some functions such as $r \cos^2 \theta$ and $r^2 \cos^4 \theta$, only one ring is needed

in order for the rule to converge to an answer within seven decimal points of the exact value from Mathematica; however, other functions like $\cos(r \cos \theta)$ need more rings to converge to the correct answer. While s , the radius remains constant, we increased the amount of rings N to observe how doing so effected the accuracy of the Fortran integral. As expected, increasing the amount of rings, increased the accuracy of the value returned by Fortran. For a radius of four and three rings, the Fortran result is only accurate to one digit; whereas, maintaining the radius at four and increasing the amount of rings to sixteen yields a result accurate within five decimal places.

Table 1: Accuracy of Fortran circular integration implementation, using Mathematica as exact answer. $f(r, \theta)$ is function being integrated, s is radius of circle, N is number of rings.

$f(r, \theta)$	s	N	Mathematica	Fortran	difference	decimal accuracy
$r \cos^2 \theta$	1	1	1.047197551	1.047197596	-4.44526E-08	7
$r^2 \cos^4 \theta$	1	1	0.589048623	0.589048637	-1.41705E-08	7
$\cos(r \cos \theta)$	4	3	-1.65985	-1.71043631	0.050586307	0
$\cos(r \cos \theta)$	4	10	-1.65985	-1.65996507	0.000115072	3
$\cos(r \cos \theta)$	4	16	-1.65985	-1.65985887	8.8707E-06	5

3.2 Surface Generation and Interpolation Using Splines

Figure 5 shows one example of a cross section of the two dimensional surface generated by random heights and a low pass frequency filter. The discrete surface is generated from a matrix where for each element, the row it is in defines the x-position on the surface and the column defines the y-position on the surface. The value of the element defines the height at that point. The blue cross symbols on the graph represent the values of the entries in the matrix. In order to calculate the surface height at locations not given by the discrete surface, namely the points described in equations 9, 10, 11, and 12, a spline interpolates between the points. The black plus symbols are the interpolated values halfway between each of the discrete surface points. The graph serves as a visual test of whether the interpolation points seem realistic. Because the curve looks continuous and the placement of the interpolation points appear reasonable, interpolation using splines works well in this project. Many cross sections were generated, and many visual tests were performed until the confidence in results reached a sufficient level.

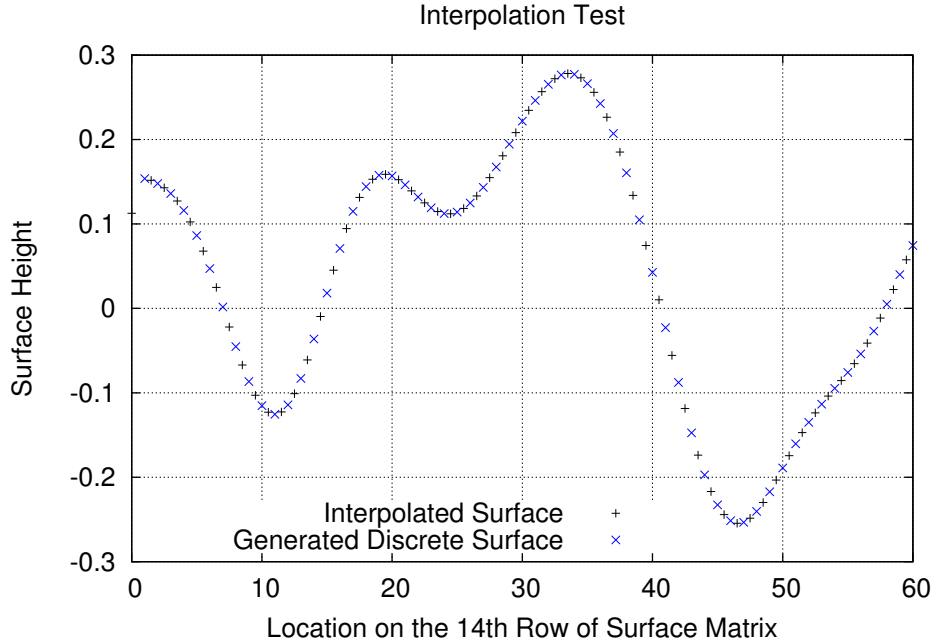
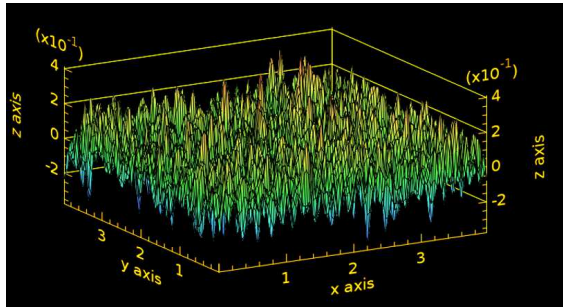


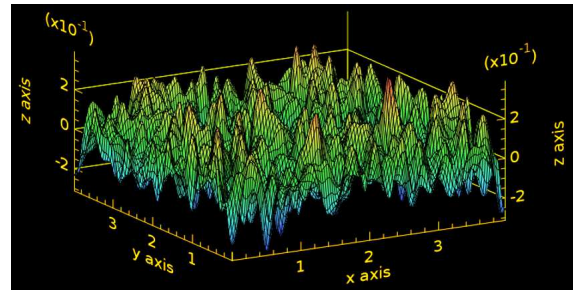
Figure 5: Visual test shows interpolated points seem reasonable.

3.3 Using Transformations for Non-Singular Calculations

Figure 6 demonstrates the effectivity half Gaussian filter used to eliminate higher spatial frequencies from the random generated surface. The z axis represents height and the units of the axes are in wavelengths. The surfaces are plotted on the same axes and scales. Before filtering, the curvatures in the surface are closer to each other, and after filtering, the curvatures smoothen out and spread apart. The filtering effects the surface as expected because eliminating high spatial frequencies, which refers to how often curvatures appear in a surface, should reduce the amount of curves in the surface.



(a) Before filter



(b) After filter

Figure 6: Randomly generated surface before and after half Gaussian filter. Height on z-axis. Units in wavelengths. Surface is smoother after filtering because higher spatial frequencies are reduced.

The splines allowed for calculations of the entries of the impedance matrix and for in-

tegrating over the product of the Greene's function and the surface Jacobian over singular patches. A Fortran module implements the transformations required by calculating the integral over singular patches, and its results agree with a Mathematica notebook that is expected to return the same results.

One method to develop the necessary transforms to eliminate the singularity in each singular patch and integrate involved a series of transformations including shifting, rotating, and shearing linear transformations for only triangle 4 in Figure 7.

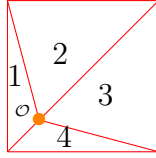


Figure 7: This is how a square is divided into triangle for one of the singularities on a patch. Each of the triangles must be transformed into standard right triangles with their singular vertex at the origin.

In Figure 7, the singularity has already been shifted to the origin o . Next the triangle was rotated by $\frac{3\pi}{4}$ radians using the rotation matrix

$$R = \begin{pmatrix} \cos \frac{3\pi}{4} & -\sin \frac{3\pi}{4} \\ \sin \frac{3\pi}{4} & \cos \frac{3\pi}{4} \end{pmatrix} \quad (27)$$

which places the shortest side of the triangle on the x-axis. Next a horizontal shearing transformation

$$H = \frac{1}{a} \begin{pmatrix} 1 & \sqrt{2}(1 + \frac{1}{\sqrt{6}}) \\ 0 & 1 \end{pmatrix} \quad (28)$$

moves one vertex to $x=1$ and the other to $y=0$. Finally an affine transformation

$$V = \begin{pmatrix} -\frac{3\sqrt{2}}{\sqrt{3}-3} & \frac{6-3\sqrt{2}+\sqrt{6}}{\sqrt{3}-3} \\ 0 & \sqrt{2} \end{pmatrix} \quad (29)$$

fixes the first vertex at $(0,0)$ and shifts the other two to $(1,0)$ and $(1,1)$.

To find the single matrix that applies these three transformations, we must matrix multiply them together in the opposite order the transformations are done in to find

$$A = \frac{1}{a} \begin{pmatrix} 0 & \frac{6}{\sqrt{3}-3} \\ 1 & -1 \end{pmatrix}. \quad (30)$$

The vertices of the 4th triangle are $(0,0)$, $(-\frac{a}{2} + \frac{a}{2\sqrt{3}}, -\frac{a}{2} + \frac{a}{2\sqrt{3}})$, and $(\frac{a}{2} + \frac{a}{2\sqrt{3}}, -\frac{a}{2} + \frac{a}{2\sqrt{3}})$, so we can apply A to a matrix containing these points, expecting to find the vertices of a standard right triangle,

$$\begin{pmatrix} 0 & \frac{6}{a(\sqrt{3}-3)} \\ \frac{1}{a} & -\frac{1}{a} \end{pmatrix} \begin{pmatrix} 0 & -\frac{a}{2} + \frac{a}{2\sqrt{3}} & \frac{a}{2} + \frac{a}{2\sqrt{3}} \\ 0 & -\frac{a}{2} + \frac{a}{2\sqrt{3}} & -\frac{a}{2} + \frac{a}{2\sqrt{3}} \end{pmatrix} = \begin{pmatrix} 0 & 1 & 1 \\ 0 & 0 & 1 \end{pmatrix}. \quad (31)$$

Equation 31 confirms that A does transform the vertices of triangle 4 to the vertices of a right triangle. Table 2 provides more reassurance that the transformations implemented within the Fortran program work correctly. The Fortran program returned the same values for the integration over the singular patches for the constant function $f(r, \theta) = 1$ as the Mathematica notebook.

Table 2: Sample of checking whether Mathematica and Fortran programs agree integrating over singular patches using Duffy Transform. n is the ring index and m is the arc piece index. The Mathematica and Fortran programs return the same answer.

n	m	Fortran	Mathematica
3	2	$0.0489868 + 0.0731842i$	$0.0489868 + 0.0731842i$
1	5	$0.0495319 + 0.0726653i$	$0.0495319 + 0.0726653i$
2	7	$0.0491463 + 0.0730489i$	$0.0491463 + 0.0730489i$

4 Conclusion

We have found an integration method that suits the symmetry of the reflectance problem and yields weights needed for calculating the impedance matrix entries at non-singular points. The efficient circular integration rule generally requires few rings in order to converge to the exact answer given in Mathematica. Additionally, a realistically rough surface was created. A fast Fourier transform makes the reduction of higher spatial frequencies in the randomly generated surface efficient. We have calculated the impedance matrix at non-singular points, setting us up to solve for the induced surface current and therefore the scattered electric field. Additionally, we have integrated over singular patches, allowing us to solve for weights that aid in the calculation of the scattered electric field. Future work includes the generation of an electric field and the calculation of the scattered electric field. Once this is set up, rms roughness and spatial frequency can be studied as parameters that effect the reflectance of XUV electromagnetic radiation.

References

- [1] Ulf Zastra, “Innovative xuv and x-ray plasma spectroscopy to explore warm dense matter,” dissertation, Friedrich-Schiller University, Jena, 1980.
- [2] Brian E. Newman, “XUV free-electron laser-based projection lithography systems,” *Proc. SPIE*, vol. 1343, p. 214, 1991.
- [3] Robert G. Brown, “Green’s function for the Helmholtz equation,” <https://webhome.phy.duke.edu/~rgb/Class/phy319/phy319/node74.html>, December 2007, (accessed 20 June 2018).
- [4] DLMF, “NIST digital library of mathematical functions,” <http://dlmf.nist.gov/3.5#x,Release1.0.15of2017-06-01>, June 2017, (accessed 10 July 2018).
- [5] R. Steven Turley, “Circular integration region,” <http://scholarsarchive.byu.edu/cgi/preview.cgi?article=2991&context=facpub>, August 2017, (accessed 17 Aug 2018).
- [6] M. E. M. G.E.P. Box, “A note on the generation of random normal deviates,” *Ann. Math. Stat*, vol. 29, pp. 610–611, 1958.
- [7] R. Steven Turley, “2d surface creation using Intel MKL,” <http://scholarsarchive.byu.edu/cgi/preview.cgi?article=2990&context=facpub>, August 2017, (accessed 17 Aug 2018).
- [8] Spencer Thevenin, “Effects of roughness on reflection of monochromatic light,” <https://www.physics.byu.edu/thesis>, April 2017, (accessed 10 June 2017).
- [9] N. S. S.E. Mousavi, “Generalized Duffy transformation for integrating vertex singularities,” <http://dilbert.engr.ucdavis.edu/~suku/quadrature/duffyquadrature.pdf>, unpublished paper.